



ELSEVIER

Earth and Planetary Science Letters 203 (2002) 105–116

EPSL

www.elsevier.com/locate/epsl

Constraints on the dynamics of mantle plumes from uplift of the Hawaiian Islands

Shijie Zhong^{a,*}, A.B. Watts^b

^a *Department of Physics, University of Colorado at Boulder, Boulder, CO 80309-0390, USA*

^b *Department of Earth Sciences, Oxford University, Oxford OX1 3PR, UK*

Received 23 April 2002; received in revised form 16 July 2002; accepted 16 July 2002

Abstract

The ~ 0.2 mm/yr uplift of Hawaiian islands Lanai and Molokai and Hawaiian swell topography pose important constraints on the structure and dynamics of mantle plumes. We have formulated 3-D models of mantle convection to investigate the effects of plume–plate interactions on surface vertical motions and swell topography. In our models, the controlling parameters are plume radius, excess plume temperature, and upper mantle viscosity. We have found that swell height and swell width constraints limit the radius of the Hawaiian plume to be smaller than 70 km. The additional constraint from the uplift at Lanai requires excess plume temperature to be greater than 400 K. If excess plume temperature is 400 K, models with plume radius between 50 and 70 km and upper mantle viscosity between 10^{20} and 3×10^{20} Pa s satisfy all the constraints. Our results indicate that mantle plume in the upper mantle may be significantly hotter than previously suggested. This has important implications for mantle convection and mantle melting. In addition to constraining plume dynamics, our models also provide a mechanism to produce the observed uplift at Lanai and Molokai that has never been satisfactorily explained before.

© 2002 Elsevier Science B.V. All rights reserved.

Keywords: mantle plumes; rheology; dynamic loading; topography; lithosphere; Hawaii island; island arcs

1. Introduction

Vertical motions of the Earth's surface in response to surface loads and mantle buoyancy forces place fundamental constraints on the rheology and dynamics of the mantle. One of the best known localities where these two processes inter-

act is the Hawaiian Islands in the Central Pacific Ocean. Here, a deep mantle plume beneath the Pacific plate has generated a chain of volcanic oceanic islands that progressively increase in age away from Hawaii Island.

Radiometric dating of submerged coral reefs [1] and sub-aerial lavas [2] indicate that despite its great height, Hawaii Island has subsided ~ 1.2 km over the last 450 kyr at a rate of $\sim 2.6 \pm 0.4$ mm/yr [1]. Lanai, ~ 225 km northwest of Hawaii (Fig. 1), however, has experienced up to 50 m of uplift in the last ~ 250 kyr at rates of ~ 0.20 mm/yr, according to studies on coral de-

* Corresponding author. Tel.: +1-303-735-5095;
Fax: +1-303-492-7935.
E-mail address: szhong@anquetil.colorado.edu (S. Zhong).

posits [3] and stratigraphic relationships within the deposits [4]. Slightly smaller rates have been suggested for the neighboring island of Molokai [3]. Oahu, at a distance of ~ 340 km from Hawaii (Fig. 1), has also been uplifted in the last 500 kyr but, at ~ 5 times smaller rates [3,5]. The main source of uncertainties of the uplift rates may be related to dating the deposits that has $\sim 15\%$ errors [3].

Previous workers have attributed the subsidence at Hawaii and uplift at Lanai, Molokai and Oahu to flexural loading at Hawaii Island. Moore [6], for example, attributed the subsidence at Hawaii to successive volcanic loads which flexed the underlying Pacific oceanic crust downwards. Watts and ten Brink [5], using a model developed earlier by McNutt and Menard [7] at isolated oceanic volcanoes, showed that the subsidence of Maui and the uplift at Oahu could be attributed to its location in Hawaii's flexural depression and bulge respectively. Griggs and Jones [3] extended the model to Lanai and Molokai, although they did not show that the model could explain the uplift observed at these islands.

The Hawaiian Islands are superimposed on a ~ 1000 km wide, ~ 1.5 km high, topographic swell [8]. It is generally agreed that the islands and swell result from the interaction of an ascending mantle plume with the moving Pacific plate [9–12]. The islands form by decompression melting of plume materials [12–14] while the swell is supported dynamically by buoyancy forces derived from the plume. Because islands are superimposed on their crest, it is difficult, however, to use the bathymetric observations to isolate the Hawaiian swell. However, profiles constructed from shipboard bathymetry grids (e.g., Fig. 1) suggest that the swell reaches its peak height, ~ 225 – 300 km 'downstream' of Kilauea, Hawaii Island. Similar results were obtained by Wessel [15] who used a 'super Gaussian' filtering technique to isolate the swell. The Hawaiian swell should influence the vertical motion history of Lanai, Molokai, and Oahu, as these islands ride the swell and move with the Pacific plate away from Hawaii Island.

The main objective of this paper is to study the effects of plume–plate interactions on the vertical

motion of Hawaiian Islands. First, we will argue that flexural loading at Hawaii Island cannot produce sufficient amount of uplift at Lanai and Molokai to explain the observations. Second, with 3-D finite element models of dynamic plume–plate interactions, we will argue that the uplift at Lanai and Molokai can be explained as a consequence of an ascending plume below Hawaii Island sheared by a moving Pacific plate. The observed uplift rates constrain the excess plume temperature to be greater than 400 K and plume radius to be less than 70 km. Finally, we will discuss the implications of our results for mantle melting and mantle convection.

2. Vertical motion from flexural loading at Hawaii Island

In this section, we will demonstrate that loading at Hawaii Island cannot produce the observed uplift at Lanai and Molokai, different from what has been proposed before [3]. We use flexure models to study vertical motions of Hawaiian islands caused by loading at Hawaii Island. Our flexure models assume an axi-symmetric disc load with radius of 36 km and a unit height acting on an incompressible elastic plate with a Young's modulus of 10^{11} Pa but different elastic thickness. The models are similar to that in [16]. We assume the axi-symmetry because the relevant load is the Hawaii Island that displays a high degree of axi-symmetry. Fig. 2 shows the flexure and vertical motions that would be expected at Lanai, Molokai and Oahu due to flexural loading at Hawaii Island. The calculations show that flexural loading causes a bulge at a distance that increases with elastic plate thickness T_e (Fig. 2a). The vertical motion rates are directly proportional to the flexure or displacement for steady-state loading process. The vertical rates are scaled such that the subsidence rate at the submerged coral reefs on Hawaii Island's north–west flank matches the observed rate of 2.6 mm/yr (Fig. 2b). Uplift rates of up to ~ 0.05 mm/yr are predicted at Lanai for $T_e = 25$ km, but the uplift turns into subsidence for $T_e > 29$ km. Similar uplift rates are predicted at Molokai, but the transition from uplift to sub-

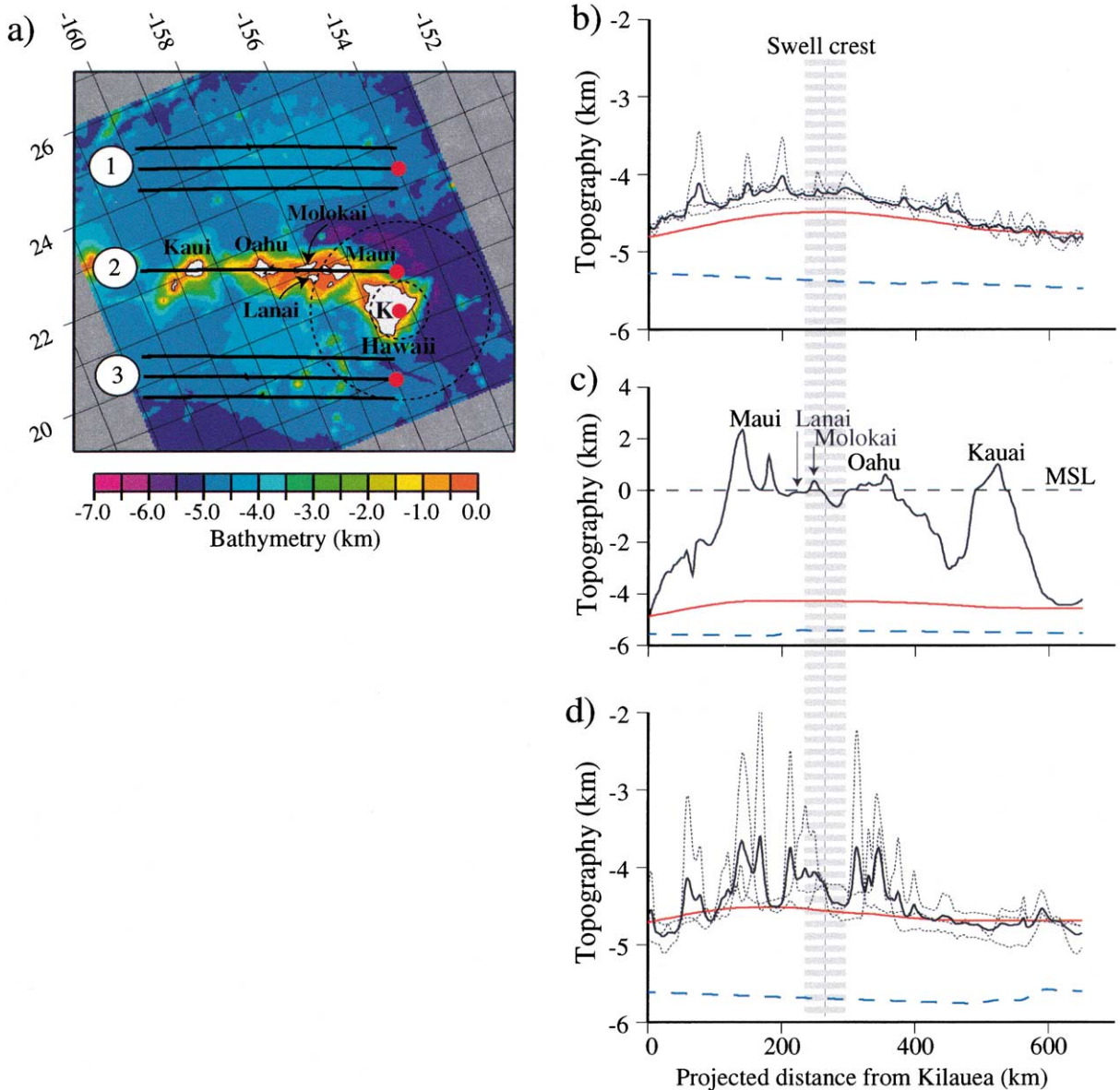


Fig. 1. Bathymetry of the Hawaiian Islands region based on shipboard data. (a) Bathymetry image. An oblique Mercator projection with the pole at -112°E , 69°N is used. Thick solid lines show the locations of the bathymetry profiles shown in (b–d). Inner dashed ring indicates the approximate extent of the load of Hawaii assumed in the elastic plate (flexure) model. Outer dashed ring is the approximate position of the flexural node for elastic plate thickness $T_e = 25$ km. (b) Bathymetry profiles (thin dotted lines) of the Hawaiian swell to the north of the islands and their average (thick solid line). (c) Bathymetry profile along the Hawaiian volcanic chain (thick solid line). (d) Bathymetry profiles (thin dotted lines) of the Hawaiian swell to the south of the islands and their average (thick solid line). In (b–d), thick red line indicates a median filter of the bathymetry/topography with filter wavelength of 500 km, and thick dashed line indicates the predicted depth of the seafloor based on a cooling plate model.

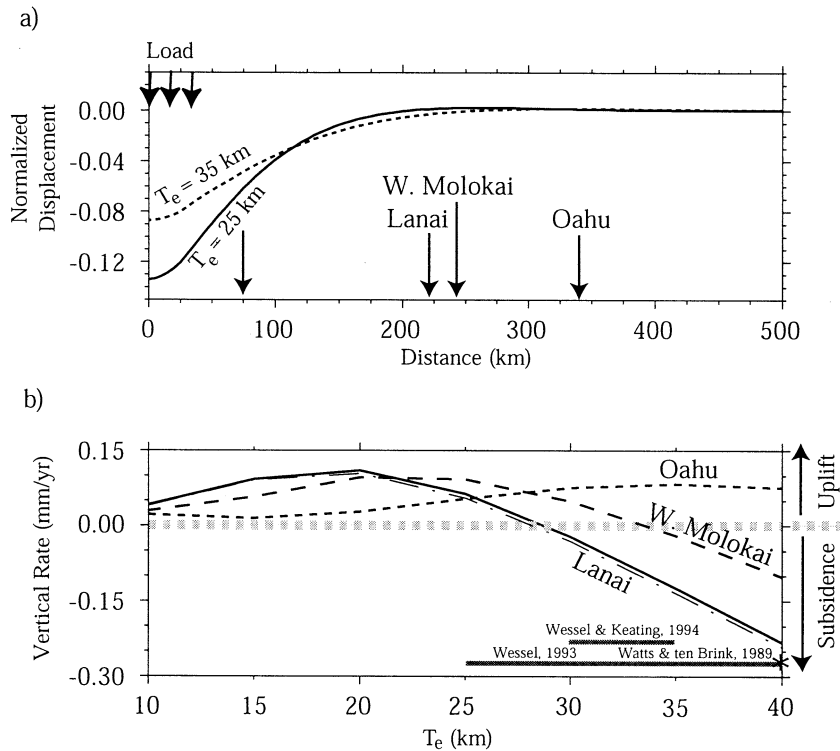


Fig. 2. Predicted flexure due to volcanic loading at Hawaii Island. (a) Flexure (normalized for load height) caused by a disk load with radius 36 km that is emplaced on an elastic plate with $T_e = 25$ km (solid line) and 35 km (dashed line). (b) Vertical motion rates at Lanai, Molokai and Oahu for different values of T_e . The rates are scaled such that the subsidence rate at the submerged coral reefs on the Hawaii Island's north-west flank (a distance of 75 km from the load center) corresponds to the observed rate of 2.6 mm/yr. The thin dash-dot line in (b) is for the rates for Lanai for load radius 50 km.

sidence occurs at the higher T_e of 34 km. Oahu is in a region of uplift, irrespective of T_e .

Since the observed T_e based on seismic and gravity modeling is in the range 25–40 km [5,17,18] with smaller T_e (~ 25 –30 km) beneath the individual islands [17], our models indicate uplift rates at Lanai of 0.05 mm/yr or less. These rates are significantly smaller than the observed uplift rates of ~ 0.2 mm/yr [3,4]. We found that increasing the load radius to 50 km generally results in $\sim 10\%$ change in the predicted rates (Fig. 2b). Therefore, flexural loading at Hawaii Island is apparently unable to explain the observed uplift of 'downstream' islands such as Lanai.

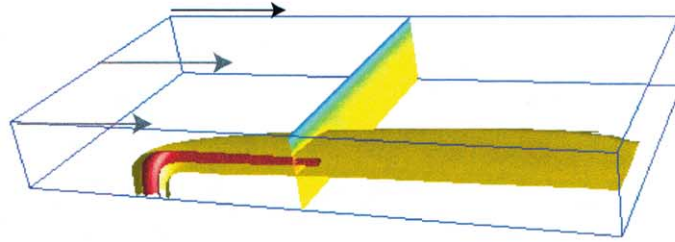
Sonar surveys suggest that the Hawaiian Islands are associated with large-scale sector collapses which have generated debris avalanches that

have traveled over the Pacific seafloor for up to a few hundred km [19]. The removal of large volumes of material from the island flanks is significant because it might uplift of the volcanic edifice that remains. However, as Smith and Wessel [20] have shown using 3-D flexural unloading models, the predicted uplift at Lanai is small ($< \sim 8$ m) and therefore is unable to contribute significantly to the observed uplift.

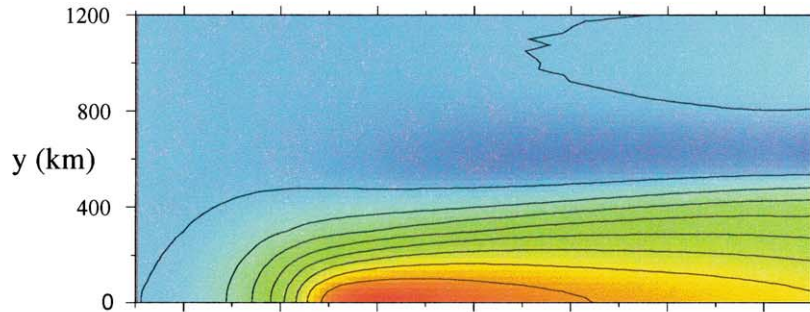
3. Vertical motion from dynamic plume–plate interactions

Our loading models suggest that flexure due to volcanic loading at Hawaii Island may only explain one fourth (or ~ 0.05 mm/yr) of the uplift at Lanai. Here we suggest that plume–plate inter-

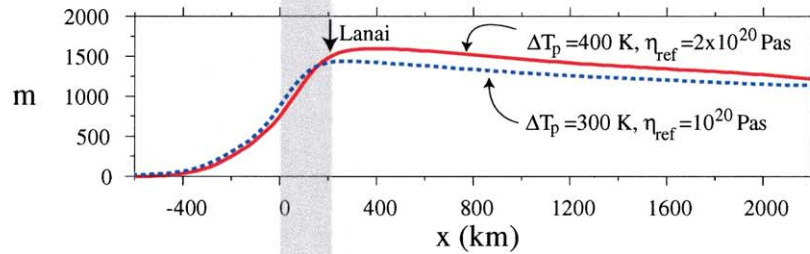
a) Thermal structure



b) Swell planform



c) Swell height



d) Vertical uplift rate

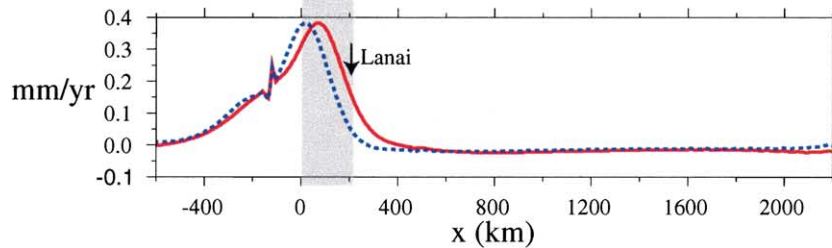


Fig. 3. 3-D thermal structure and topography from a plate–plume interaction model. (a) Thermal structure for a model with $R_p = 65$ km, $\Delta T_p = 400$ K, and $\eta_o = 2 \times 10^{20}$ Pa s. Arrows indicate the direction of plate motion. The two constant temperature surfaces are for 1400 (yellow) and 1600°C (red), respectively. (b) The corresponding planform of the swell topography (contour interval = 200 m), (c) dynamic topography of the swell crest, and (d) vertical uplift rate of the swell crest for the model in (a). Dashed lines in (c,d) are for a model that only differs from (a) by having $\Delta T_p = 300$ K and $\eta_o = 10^{20}$ Pa s.

actions are the primary cause of the uplifts at Lanai and Molokai. We have tested this possibility by constructing 3-D finite element models of mantle convection with plume–plate interactions.

3.1. Models of plume–plate interactions

Our 3-D cartesian models of mantle convection are similar to those in [11] (Fig. 3a). The model box is 400 km deep, 1600 km wide and 3200 km long in the direction of plate motion. The bottom boundary at a depth of 400 km is assumed to have zero horizontal velocity and vertical stress, and the latter permits vertical flow through it. The bottom boundary is assumed to be at a uniform temperature of 1350°C, except in a circular region which simulates an ascending mantle plume. The surface is assumed to be at a constant temperature (0°C) and to have the same horizontal velocity (86 mm/yr) as the absolute motion of the Pacific plate. Flow-through boundary conditions are applied to the left and right side-walls of the box. The inflow from the left side-wall has a fixed temperature profile derived from a half-space cooling model for a 80 Ma old lithosphere, and outflow at the right side-wall has a zero temperature gradient. Reflecting boundary conditions are applied to the front side-wall and rear side-walls are stress-free.

The circular region on the bottom boundary that simulates a plume is located at 800 km distance from the inflow boundary and maintains a temperature anomaly $\Delta T = \Delta T_p \exp(-r^2/R_p^2)$, where R_p and ΔT_p are the radius and excess temperature of the plume and r is the distance from the plume center. Our models assume a temperature-dependent Newtonian rheology $\eta = \eta_o \exp[E/R(1/T - 1/T_b)]$, where E is activation energy, η_o and T_b are background viscosity and background temperature in the upper mantle, respectively, and R is the gas constant. In this study, E is taken as 120 kJ/mol, T_b is 1350°C, and η_o varies from 5×10^{19} to 4×10^{20} Pa s. In our calculations, we will primarily vary η_o , R_p , and ΔT_p while keeping other model parameters fixed (Table 1).

The calculations are based on the finite element code CITCOM [21] with various extensions including parallel computing [22]. Our models

have ~ 10 km vertical resolution and 5 km horizontal resolution near the plume. We integrate our models for a sufficiently large number of time steps to get a steady-state solution. Our models do not display significant time-dependence or boundary layer instabilities. Boundary layer instabilities may be expected for models with large activation energy [23]. Our models use activation energy of 120 kJ/mol that is constrained by observed flexural rigidity near seamounts [16]. This activation energy is smaller than those deduced from laboratory studies on mantle rocks. However, with a Newtonian rheology, activation energy larger than 120 kJ/mol may predict too large flexural rigidity or too thick elastic plate near the seamounts than observed [16].

We have made a number of simplifications that deserve some discussions. (1) The effects of melting on buoyancy and temperature are not considered. A recent study suggests that they may increase swell topography by 25% [14]. We believe that such relatively small effects of melting will not change our basic results. (2) The bottom boundary in our models is open, similar to [11,23]. Previously, 3-D models of plume–plate interactions have been formulated for the entire mantle to study the generation of plumes [24]. It is, however, computationally difficult to use such models for our study in which we need to resolve plumes with radius of ~ 50 km. We have addressed this issue with calculations for larger box depth that indicate that our results are not sensitive to box depth.

3.2. Results

Fig. 3 shows the steady-state thermal structure,

Table 1
Parameters for plume–plate interaction models

Parameter	Value
Activation energy	120 kJ/mol
Thermal diffusivity	10^{-6} m ² s ⁻¹
Coefficient of thermal expansion	3.5×10^{-5} K ⁻¹
Mantle density	3300 kg m ⁻³
Water density	1000 kg m ⁻³
Mantle temperature	1350°C
Depth of model box	4×10^5 m
Surface plate motion	86 mm/yr

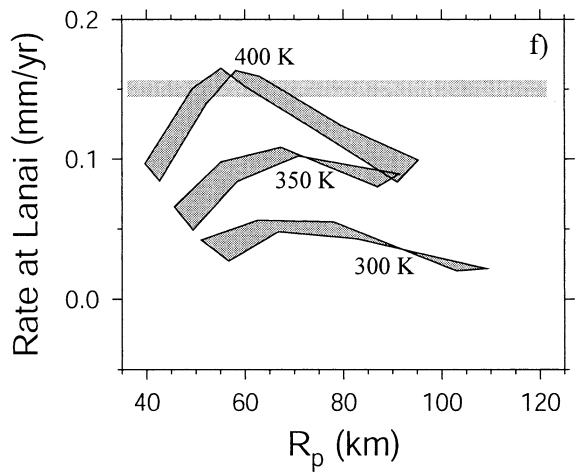
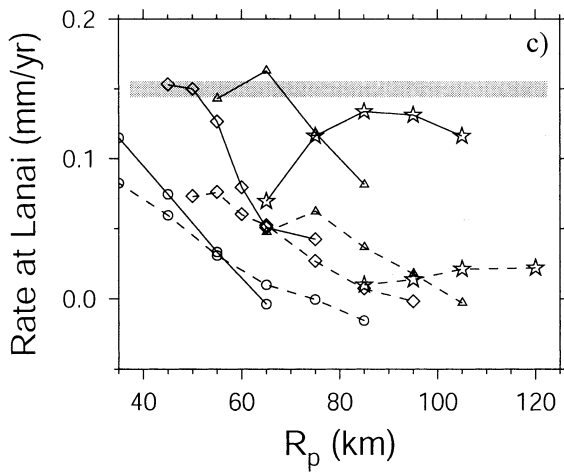
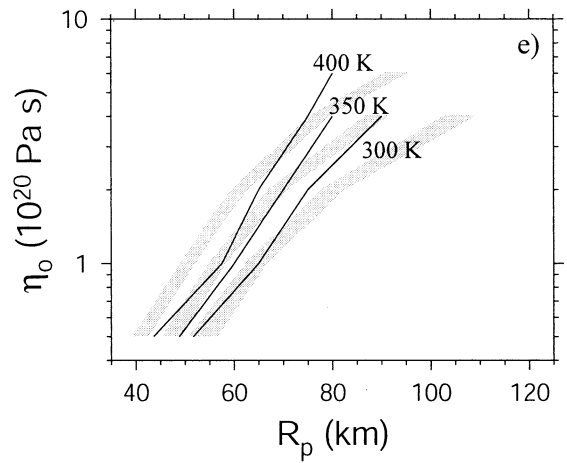
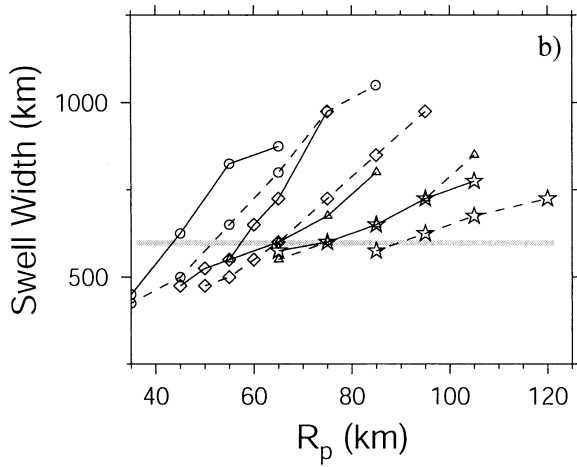
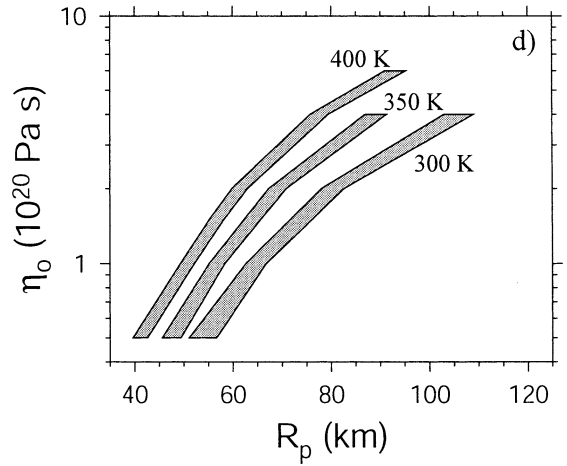
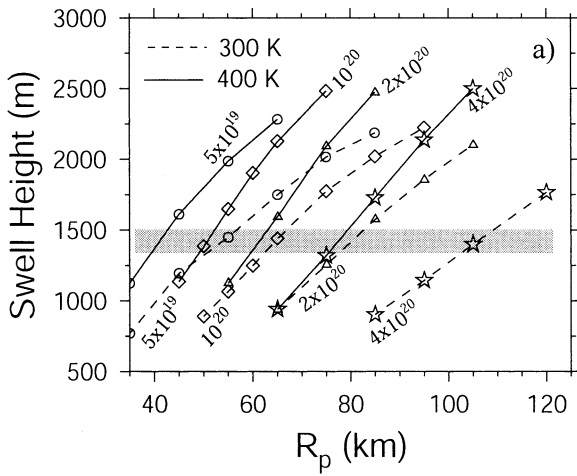
topography, and uplift rates for a model run with $R_p = 65$ km, $\Delta T_p = 400$ K, and $\eta_o = 2 \times 10^{20}$ Pa s. The topography excludes the effects of lithospheric cooling, following that in [11]. The figure shows that the temperature is characterized by a thermal plume and a thin thermal sheet below the moving plate. The plume buoyancy flux is 3980 kg/s, consistent with previous estimates [11]. The plume produces a swell with a maximum height of ~ 1590 m and a half-width of ~ 600 km at the plume center (Fig. 3b,c). The plume center is defined here as the point in the ascending plume where the flow reaches the melting point. The swell crest is located ~ 300 km ‘downstream’ of the plume center. The swell width is defined as the distance to the swell axis from where topographic gradient decreases to 10^{-4} along the topographic profile perpendicular to the plate motion at plume center. The swell width is generally $\sim 10\%$ larger if we use the minimum topography along the perpendicular topographic profile as a criterion. However, in some cases a stable minimum topography is hard to locate, due to some weak time-dependence at the edge of the spreading plume. While the predicted half-width for the swell is consistent with the observed (~ 600 km in [15]), the predicted maximum swell height along the swell axis is ~ 250 m larger than that inferred from the bathymetry profiles ~ 200 km off the volcanic chain [8]. However, because the Hawaiian Islands obscure the true shape of the swell crest, we think that a maximum swell height between 1350 and 1500 m is a reasonable estimate.

With the swell topography, we compute the uplift rate by multiplying the plate velocity with the topographic gradient in the direction of plate motion. As Fig. 3c,d shows, an island that forms above a plume center experiences uplift as it ‘rides’ the swell crest. At Lanai, which is now ~ 220 km from the plume center, uplift rates as large as 0.15 mm/yr are predicted by the models. The uplift rates at Molokai are slightly smaller at 0.11 mm/yr. However, the vertical rates at Oahu are insignificantly small (Fig. 3d), because of the relatively large distance from the plume. Because Molokai is very close to Lanai and the predicted uplift rates are similar, we will focus on uplift rates at Lanai.

We have examined the sensitivity of the calculated uplift rates to model parameters with more than 70 cases. The predicted uplift rates at Lanai, U_{Lanai} , are sensitive to R_p , ΔT_p , and η_o . However, the model predictions were found to depend weakly on the box size. For example, increasing box depth in Fig. 3 to 600 km only results in $\sim 10\%$ variations in the maximum swell height and uplift rates. However, the increasing box depth results in 35% increase in plume buoyancy flux, suggesting that plume buoyancy flux is sensitive to box depth [11].

Fig. 4a,b shows that the model swell height and swell width have similar dependence on R_p , η_o and ΔT_p in that swell height and swell width increase with increasing R_p and ΔT_p and decreasing η_o . For models with a given ΔT_p , only certain combinations of R_p and η_o reproduce the observed swell height (i.e., between 1350 and 1500 m) (Fig. 4a) and swell width at the plume center (i.e., 600 km) (Fig. 4b). Fig. 4d,e shows those R_p and η_o for different ΔT_p that reproduce the observed swell height and swell width, respectively. For ΔT_p between 300 and 400 K, only models with $R_p < 70$ km and $\eta_o < 3 \times 10^{20}$ Pa s satisfy both swell height and swell width constraints, and for larger R_p the two sets of curves for swell height and swell width diverge rapidly (Fig. 4b). However, it is difficult to use swell height and swell width constraints to further circumscribe parameter space for R_p , η_o and ΔT_p , because for $R_p < 70$ km and $\eta_o < 3 \times 10^{20}$ Pa s, swell height and swell width have similar dependence on R_p , η_o and ΔT_p . This is not surprising considering that swell height and swell width are not entirely independent and that they both increase with plume buoyancy flux [11] which should increase with R_p and ΔT_p but decrease with η_o .

The uplift rate at Lanai, U_{Lanai} , in general also increases with ΔT_p (Fig. 4c). However, different from swell height and swell width, U_{Lanai} peaks at a certain R_p for a given η_o (Fig. 4c). These models satisfying the swell height constraint produce very different U_{Lanai} (Fig. 4c,f). For $\Delta T_p = 300$ K, the maximum possible U_{Lanai} is ~ 0.05 mm/yr that occurs for $R_p = 65$ km and $\eta_o = 10^{20}$ Pa s (Figs. 4f and 3d), while for



$\Delta T_p = 400$ K, U_{Lanai} is greater than 0.15 mm/yr for R_p between 50 and 70 km (Fig. 4f) and the corresponding η_o between 10^{20} and 3×10^{20} Pa s. Other parameter pairs such as $R_p \sim 40$ km and $\eta_o \sim 5 \times 10^{19}$ Pa s for $\Delta T_p = 400$ K or $R_p < 70$ km and $\eta_o < 3 \times 10^{20}$ Pa s for $\Delta T_p = 350$ K satisfy the swell height and swell width constraint (Fig. 4e) but, predict $U_{\text{Lanai}} < 0.1$ mm/yr (Fig. 4f). This indicates that plume excess temperature ΔT_p is required to be greater than 400 K in order to produce the observed U_{Lanai} (i.e., > 0.15 mm/yr).

4. Discussions and conclusions

We have demonstrated that both flexural loading and plume–plate interactions contribute to the vertical motions that have been observed in the Hawaiian Islands. At Hawaii Island, the subsidence caused by loading (Fig. 2b) clearly dominates the uplift due to plume–plate interactions (~ 0.35 mm/yr in Fig. 3d). However, volcanic loading contributes only a small amount (~ 0.05 mm/yr) to the uplift of ‘downstream’ islands such as Lanai (Fig. 2b). Here, plume–plate interactions are more important (Fig. 3d). The models in Fig. 4 show that the uplift from plume–plate interactions depends on not only plume radius R_p and upper mantle viscosity η_o , but also the excess plume temperature ΔT_p . However, for $\Delta T_p = 300$ K the maximum possible U_{Lanai} is ~ 0.05 mm/yr (Fig. 4f), which is too small to account for the observed rate of ~ 0.2 mm/yr. ΔT_p needs to be at least 400 K to match the observations (Fig. 4f), provided that flexural loading contributes less than 0.05 mm/yr to the uplift rate at Lanai (the rate predicted from a model with uniform T_e of 25 km). At Oahu and other islands further ‘down-

stream’, dynamic topography has an insignificant influence on vertical motions (Fig. 3c). However, at Oahu flexural loading predicts rates of 0.04 and 0.07 mm/yr (Fig. 2b) which are consistent with observations [3].

We have shown that in conjunction with observed swell height and swell width, the uplift rate at Lanai poses strong constraints on plume dynamics. Swell height, swell width, and uplift rates are most sensitive to three parameters: R_p , ΔT_p , and η_o . Swell height (i.e., 1.35–1.5 km) and swell half-width (i.e., 600 km) constraints require $R_p < 70$ km (Fig. 4e). However, for $R_p < 70$ km and a given ΔT_p , models with parameters R_p and η_o that satisfy the swell height constraint also satisfy the swell width constraint equally well (Fig. 4e). This implies that swell height and swell width no longer provide independent constraints for $R_p < 70$ km. The uplift rate at Lanai introduces additional constraints that require $\Delta T_p \geq 400$ K, and if $\Delta T_p = 400$ K, then we have $50 \text{ km} \leq \Delta T_p \leq 70 \text{ km}$ and $10^{20} \text{ Pa s} \leq \eta_o \leq 3 \times 10^{20} \text{ Pa s}$.

The uplift rates at ‘downstream’ islands provide constraints on plume dynamics, because the uplift rates depend on plate–plume coupling and also plume buoyancy. The uplift rates are determined by topographic slope that depends not only on the maximum swell height but also on the location of swell maximum with respect to the plume. For Lanai and Molokai to experience uplift, our models suggest that they need to be located between the plume and the swell maximum (Figs. 3c,d). Although the Hawaiian volcanoes obscure the swell crest, there is an indication in bathymetric profiles at ~ 200 km distance from the volcanic chain that the swell maximum may be located further ‘downstream’ from Hawaii than Lanai and Molokai (Fig. 1).

←
 Fig. 4. Sensitivity of the model calculations to ΔT_p , R_p , and η_o . (a) Predicted swell height for different values of R_p , η_o and ΔT_p (dashed lines for 300 K and solid lines for 400 K). The gray line indicates a swell height of 1.5 km. The symbols circle, diamond, triangle, and star are for η_o of 5×10^{19} , 10^{20} , 2×10^{20} , and 4×10^{20} Pa s, respectively, and each symbol represents a single model run. (b) Predicted swell width and (c) predicted vertical motion rate at Lanai Island for the same models in (a). Symbols and lines are as in (a). (d) Models with parameters of R_p , η_o and ΔT_p that produce swell height between 1.35 and 1.5 km and (e) swell width of 600 km. (f) Predicted vertical motion rate at Lanai Island for those models with different values of R_p and ΔT_p in (d). As finite element models may not exactly produce desired swell height and width (e.g., a,b), (d–f) are based on interpolation of results from (a–c) for $\Delta T_p = 300$ and 400 K and from model runs for $\Delta T_p = 350$ K.

The location of the swell maximum with respect to the plume depends on distribution of mantle buoyancy. The mantle buoyancy consists of two parts: the vertical plume conduit and the horizontal thermal sheet (Fig. 3a), and the swell topography is the sum of dynamic topography resulting from each of these two structures. While the plume conduit produces topography that peaks directly above the plume, it is the thermal sheet that causes the ‘downstream’ offset of swell maximum with respect to the plume. This offset depends on relative importance between plate’s shear force that controls the horizontal thermal sheet and the plume buoyancy (i.e., R_p and ΔT_p). With similar plume buoyancy flux and R_p , the two cases in Fig. 3c produce similar topography. However, the peak topography from the case with smaller viscosity (i.e., smaller shear from the plate) is closer to the plume center and this leads to significantly smaller U_{Lanai} (Fig. 3c,d). This also helps understand why U_{Lanai} peaks at certain R_p in Fig. 4c,f. In order to maintain similar plume buoyancy flux or swell height, η_o (i.e., plate’s shear force) needs to increase with R_p (Fig. 4d). Therefore, as R_p increases the increasing plate shear causes the topography to peak at a larger distance from the plume head and a larger U_{Lanai} (Fig. 4f). However, when R_p is sufficiently large, compensation of the buoyancy in the plume conduit becomes so effective that it starts to control the location of the peak topography. In this situation, increasing R_p tends to move the peak topography closer to the plume and reduce U_{Lanai} (Fig. 4f).

In addition to providing an explanation for uplift of the Hawaiian Islands, our study has implications for dynamic topography, the dynamics of mantle plumes, and mantle melting. Although it has long been suggested that mantle dynamic processes including subduction can cause submergence or/and emergence of continents at large temporal (10–100 Ma) and spatial (>2000 km) scales [25,26], we believe that vertical motions of the Hawaiian Islands in the last 250 kyr suggest that this process may operate at much smaller scales.

Our estimate of >400 K for the excess plume temperature is significantly larger than the

~280 K estimated from a previous study by comparing melting production rate, geoid and topography at Hawaii with predictions from axis-symmetric and isoviscous mantle convection models [13]. However, recent studies suggest that this estimate of 280 K may not be well constrained. These include: (1) The melt production rate at Hawaii is recently estimated to be 70% larger [12] than used in [13]. This suggests that a larger ΔT_p is needed to enhance the melt production rate. (2) The geoid/topography ratio for the Hawaiian swell after eliminating seamounts effects may be twice [27] of that used in [13]. In addition, more realistic convection models based on a 3-D geometry and temperature-dependent viscosity with similar ΔT_p [11,14] produce significantly different geoid/topography ratios than from isoviscous mantle convection models.

Several other lines of evidence support the larger estimates of ΔT_p inferred in our study. These include: (1) Recent theoretical and laboratory studies that indicate significant decrease in melt productivity for fractional melting [28,29]. This implies a larger ΔT_p than in [13] so as to produce the same amount of melt at Hawaii [14]. (2) Seismic observations that reveal a melting zone at depths of 130–170 km below Hawaii [30]. While melting at the 130 km depth suggests $\Delta T_p \sim 300$ K for the Hawaiian plume [30], $\Delta T_p \sim 400$ K is required to initiate melting at the bottom of the melting zone (i.e., 170-km depth). (3) We note that the larger ΔT_p is consistent with that from other models of mantle convection. The excess temperature in a plume in the upper mantle depends on the plume buoyancy flux and, hence, initial excess temperature that it acquires from the bottom thermal boundary layer [31]. For the Hawaiian plume, an excess temperature of $\Delta T_p = 280$ K in the upper mantle implies only 500 K initial excess temperature in the lower mantle, and this is much smaller than that predicted for a whole mantle model [31]. Although a bottom chemical layer with dense material may reduce the temperature for plumes originating from this layer [32], recent layered mantle models predict significantly larger ΔT_p in the upper mantle [33]. (4) Recent studies on geodynamo suggest significantly larger core heat flux than previously

believed [34]. The larger core heat flux may imply larger ΔT_p .

An upper-mantle viscosity η_o of $\sim 2 \times 10^{20}$ Pa s from our study is consistent with that estimated for the sub-lithospheric mantle from lateral spreading of the Hawaiian swell root [12]. Phipps-Morgan et al. [12] suggested that in order to preventing the Hawaiian swell root from spreading two rapidly, significant coupling between the Pacific plate and the swell root is required and the viscosity of the swell root needs to be 3×10^{20} Pa s. In [12], the swell root is considered as melt residue derived from melting the plume, and the swell root is compositionally buoyant and more viscous than the ambient mantle. Our study does not consider the possible influences of melting on buoyancy and viscosity. The effects of melting need to be examined in future studies.

Acknowledgements

We would like to thank G. Ito and P. van Keken for their careful reviews. S.Z. thanks M. Zuber for her support. This study is funded by David and Lucile Packard Foundation and NSF under Grant number EAR-0134939. [RV]

References

- [1] J.G. Moore, D.A. Clague, Volcano growth and evolution of the island of Hawaii, *Geol. Soc. Am. Bull.* 104 (1992) 1471–1484.
- [2] J.G. Moore, B.L. Ingram, K.R. Ludwig, D.A. Clague, Coral ages and island subsidence, Hilo drill hole, *J. Geophys. Res.* 101 (1996) 11599–11605.
- [3] R.W. Grigg, A.T. Jones, Uplift caused by lithospheric flexure in the Hawaiian Archipelago as revealed by elevated coral deposits, *Mar. Geol.* 141 (1997) 11–25.
- [4] K. Rubin, C.H. Fletcher III, C. Sherman, Fossiliferous Lana'i deposits formed by multiple events rather than a single giant tsunami, *Nature* 408 (2000) 675–681.
- [5] A.B. Watts, U.S. tenBrink, Crustal structure, flexure, and subsidence history of the Hawaiian islands, *J. Geophys. Res.* 94 (1989) 10473–10500.
- [6] J.G. Moore, Relationship between subsidence and volcanic load, Hawaii, *Bull. Volcanol.* 34 (1970) 562–576.
- [7] M.K. McNutt, H.W. Menard, Lithospheric flexure and uplifted atolls, *J. Geophys. Res.* 83 (1978) 1206–1212.
- [8] R.S. Detrick, S.T. Crough, Island subsidence, hot spots, and lithospheric thinning, *J. Geophys. Res.* 83 (1978) 1236–1244.
- [9] G.F. Davies, Oceanic bathymetry and mantle convection, 1. large-scale flow and hotspots, *J. Geophys. Res.* 93 (1988) 10467–10480.
- [10] P. Olson, Hot spots, swells and mantle plumes, in: M.P. Ryan (Ed.), *Magma Transport and Storage*, John Wiley, New York, 1990, pp. 33–51.
- [11] N.M. Ribe, U.R. Christensen, 3-Dimensional modeling of plume-lithosphere interaction, *J. Geophys. Res.* 99 (1994) 669–682.
- [12] J. Phipps-Morgan, W.J. Morgan, E. Price, Hotspot melting generates both volcanism and a hotspot swell?, *J. Geophys. Res.* 100 (1995) 8045–8062.
- [13] S. Watson, D. McKenzie, Melt generation by plumes: A study of Hawaiian volcanism, *J. Petrol.* 32 (1991) 501–537.
- [14] N.M. Ribe, U.R. Christensen, The dynamical origin of Hawaiian volcanism, *Earth Planet. Sci. Lett.* 171 (1999) 517–531.
- [15] P. Wessel, Observational constraints on models of the Hawaiian hot spot swell, *J. Geophys. Res.* 98 (1993) 16095–16104.
- [16] A.B. Watts, S. Zhong, Observations of flexure and the rheology of oceanic lithosphere, *Geophys. J. Int.* 142 (2000) 855–875.
- [17] P. Wessel, A reexamination of the flexural deformation beneath the Hawaiian islands, *J. Geophys. Res.* 98 (1993) 12177–12190.
- [18] P. Wessel, B.H. Keating, Temporal variations of flexural deformation in Hawaii, *J. Geophys. Res.* 99 (1994) 2747–2756.
- [19] J.G. Moore, D.A. Clague, R.T. Holcomb, P.W. Lipman, W.R. Normark, M.E. Torresan, Prodigous submarine landslides on the Hawaiian Ridge, *J. Geophys. Res.* 94 (1989) 17465–17484.
- [20] J.R. Smith, P. Wessel, Isostatic consequence of giant landslides on the Hawaiian ridge, *Pure Appl. Geophys.* 159 (2000) 1097–1114.
- [21] L. Moresi, M. Gurnis, Constraints on the lateral strength of slabs from three-dimensional dynamic flow models, *Earth Planet. Sci. Lett.* 138 (1996) 15–28.
- [22] S. Zhong, M.T. Zuber, L. Moresi, M. Gurnis, The role of temperature-dependent viscosity and surface plates in spherical shell models of mantle convection, *J. Geophys. Res.* 105 (2000) 11063–11082.
- [23] W.B. Moore, G. Schubert, P. Tackley, Three-dimensional simulations of plume-lithosphere interaction at Hawaiian Swell, *Science* 279 (1998) 1008–1011.
- [24] P. van Keken, C. Gable, The interaction of a plume with a rheological boundary: A comparison between two- and three-dimensional models, *J. Geophys. Res.* 100 (1995) 20291–20302.
- [25] J.X. Mitrovica, C. Beaumont, G.T. Jarvis, Tilting of continental interiors by the dynamical effects of subduction, *Tectonics* 8 (1989) 1079–1094.

- [26] M. Gurnis, Phanerozoic marine inundation of continents driven by dynamic topography above subducting slabs, *Nature* 364 (1993) 589–593.
- [27] L. Cserepes, U.R. Christensen, N.M. Ribe, Geoid height versus topography for a plume model of the Hawaiian swell, *Earth Planet. Sci. Lett.* 178 (2000) 29–38.
- [28] M.M. Hirschmann, P.D. Asimow, M.S. Ghiorso, E.M. Stolper, Calculation of peridotite partial melting from thermodynamic models of minerals and melts. III. Controls on isobaric melt production and the effect of water on melt production, *J. Petrol.* 40 (1999) 831–851.
- [29] K. Hirose, K. Kawamura, A new experimental approach for incremental batch melting of peridotite at 1.5 GPa, *Geophys. Res. Lett.* 21 (1994) 2139–2142.
- [30] X. Li, R. Kind, K. Priestley, S.V. Sobolev, F. Tilmann, X. Yuan, M. Weber, Mapping the Hawaiian plume conduit with converted seismic waves, *Nature* 405 (2000) 938–941.
- [31] M. Albers, U.R. Christensen, The excess temperature of plumes rising from the core-mantle boundary, *Geophys. Res. Lett.* 23 (1996) 3567–3570.
- [32] C.G. Farnetani, Excess temperature of mantle plumes: The role of chemical stratification across D' , *Geophys. Res. Lett.* 24 (1997) 1583–1586.
- [33] L.H. Kellogg, B.H. Hager, R.D. vanderHilst, Compositional stratification in the deep mantle, *Science* 283 (1999) 1881–1884.
- [34] D. Gubbins, D. Alfe, G. Masters, D. Price, M.J. Gillan, Can the Earth's dynamo run on heat alone? *Geophys. J. Int.* (2001), submitted.